COBEM 2023 27TH INTERNATIONAL CONGRESS OF MECHANICAL ENGENEERING

ABCM Brazilian Society of Mechanical Sciences and Engineering
27th ABCM International Congress of Mechanical Engineering
December 04-08, 2023, Florianópolis-SC, Brazil

# COB-2023-0200
# J-INTEGRAL STUDY IN HYPERELASTIC MATERIAL SUBMITTED TO A MODE I FRACTURE LOADING

**Lucas Macedo Barboza**
lucasmacedo@id.uff.br
**João Carlos Andrade de Deus Filho**
joaocadf@id.uff.br
**Luiz Carlos da Silva Nunes**
luizcsn@id.uff.br
Laboratory of Opto-Mechanics (LOM), Department of Mechanical Engineering (PGMEC-TEM), Universidade Federal Fluminense – UFF, Rua Passo da Pátria, 156, Bloco E, Sala 210, Niterói, RJ CEP 24210-240, Brazil.

***Abstract.*** *It is known that soft biological tissues can be considered hyperelastic materials. Therefore, a deeper knowledge on the behavior of hyperelastic materials subjected to different conditions and loads, enables a greater understanding of this type of tissue. Thus, it becomes possible the development of protocols for injury prevention, the creation of prostheses, and advancing treatments against chronic joint pain. The goal of this work is to analyze the J-integral in a cracked pure shear specimen of incompressible and isotropic hyperelastic material subjected to mode-I loading. The material used was a silicone rubber, and the tests were carried out in a universal tensile machine, which performed a quasi-static movement, at constant temperature. To measure the displacement and deformation fields, the Digital Image Correlation method was employed. By varying the paths and regions around the crack tip, the study revealed that the line and area J-Integral do not have similar values, due to the difference in the domain they are calculated. Additionally, this work highlights that the stresses in the loading direction significantly impact the area J-Integral results, so that other stresses can be neglected in the calculations without compromising the final outcome.*

***Keywords:*** *J-Integral, hyperelastic material, Digital Image Correlation, fracture.*

## 1. INTRODUCTION

Soft biological tissues, including skin, muscles, and cerebral gray matter exhibit an elastic non-linear relationship between stress and strain when subjected to significant deformation. The mechanical behavior of these materials can be described by the theory of hyperelasticity, i.e., they can be classified as hyperelastic materials (Khaniki et al., 2022). A better understanding of injuries and diseases requires comprehension of the mechanical behavior of these materials under different load conditions.

By utilizing elastic materials, it becomes possible to overcome anatomical barriers and reach regions that would otherwise require more invasive procedures (Kumar and Ali syed, 2020). These materials also play a significant role in surgeries and cardiac treatments, where gloves made from hyperelastic materials can be attached to the outer surface of the heart, assisting its functioning and enhancing vital functions in patients with heart failure (Horvath et al., 2018).

The field of biomedical robotics is also advancing and employing hyperelastic materials as a key component. Robotic gloves made from these materials provide patients in the process of recovering their motor skills with faster and more efficient treatment. These gloves offer smoother movements compared to less elastic materials and enable greater sensitivity when handling objects (Xiong et al., 2021).

Tendons and cartilage are examples of soft biological tissues that, when studied under different load conditions, contribute to the development of protocols for injury prevention, prostheses for individuals with mobility restrictions, and advancements in treating chronic joint pain (Cianchetti et al., 2018). Additionally, the study of the fracture of hyperelastic materials enables the creation of artificial tissues and repair materials. These materials find applications in reconstructing damaged tissues resulting from severe burns, perforations, or tears.

The presence of cracks is a key factor contributing to a decrease in the mechanical strength of structural components, which can ultimately result in failure. Fracture Mechanics, pioneered by Griffith (1921), aims to study crack propagation in structures, preventing material rupture. To analyze and quantify crack propagation, various methods have been developed over time. Irwin (1957) proposed the stress intensity factor to predict stress at the crack tip, while Wells (1963) introduced the concept of crack tip opening displacement (CTOD).

Recognizing the limitations in linear elastic fracture approaches imposed by the presence of a plastic region, Rice (1968) proposed the line J-Integral method. This method quantifies fracture toughness using a closed path around the crack tip. Li et al. (1985) further extended this concept by proposing an expression analogous to the Rice integral, utilizing

the divergence theorem to convert the volume integral to an area integral for two-dimensional problems. Few years later, Kim (1989) proposed a method based on the energy stored by the specimen during the fracture test.

The objective of this work is to carry out a study of the line Integral-J and area Integral-J methods, used for analyzing and quantifying the strain energy release rate. A comparison between both methods was done, in order to verify if they are similar. Three pure shear specimens made of silicone rubber was tested under mode-I loading. Displacement and strain fields were experimentally obtained by the Digital Image Correlation method.

## 2. EXPERIMENTS

### 2.1 Material and specimens

A liquid silicone rubber model 4-150 RTV from Moldflex was chosen to manufacture the three pure shear specimens (planar specimens) used in this study. This is a low-cost rubber vulcanized by condensation at room temperature (≅ 25°C), used in the production of flexible molds for soaps, candles, biscuits and plaster. This material exhibits good fluidity, flexibility and elongation.

For the manufacture of the pure shear specimens, a rectangular aluminum mold was used, which was supported on a flat surface in order to guarantee a constant thickness. For preparing the sample for the use of the Digital Image Correlation method, a random black pattern is applied using a spray in the central region of the specimen. To induce mode I loading on the planar specimens, a pre-crack, *a*, of 20 mm was made. The dimensions are represented in Figure 1 and their values shown in Table 1.

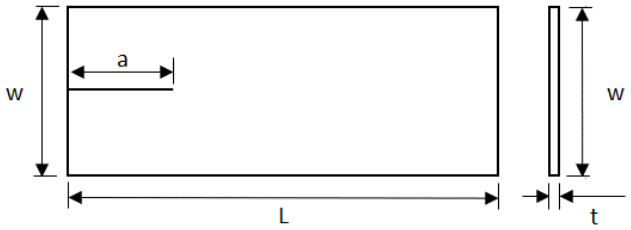


Figure 1. Representation of the pure shear specimens.

Table 1. Dimensions of the pure shear specimens

| Specimen | Length (L), mm | Width (w), mm | Thickness (t), mm |
|---|---|---|---|
| 1 | 99,76 | 49,98 | 2,54 |
| 2 | 100,36 | 50,72 | 2,46 |
| 3 | 99,62 | 49,50 | 2,38 |

### 2.2 Digital Image Correlation

One of the main challenges in the field of fracture mechanics is to understand the behavior of failures in structures subjected to different types of loads. Therefore, traditional techniques that measure local deformations and need to be attached to the material are being replaced by techniques based on images. These techniques do not require physical contact with the specimen and allow obtaining displacement fields. Techniques based on images, as the Digital Image Correlation (DIC), have been successfully developed and applied in a wide range of scientific and engineering problems, such as in the fracture mechanics and in the biomechanics (Sutton et al., 2000).

The Digital Image Correlation is an optical-numerical measurement technique, which allows to determine displacement and deformation fields on the surface of objects under varying loads (Sutton et al., 1983). This technique involves capturing images of the specimen before, during, and after deformation, which are processed using specialized software. In this technique, the preparation of the surface specimen is crucial. For this purpose, a random pattern, produced by a spray, must be inserted on specimen surface.

The Digital Image Correlation technique enables the identification of surface properties of a specimen in images captured by a digital camera, assigning coordinates to the pixels in the image. The fundamental principle behind the DIC technique involves selecting a group of points in the reference image (reference subset) and determining their corresponding positions in the deformed image (deformed subset), i.e., DIC captures images while the specimen is under load, compares them with the initial image, and computes the deformation of the specimen based on its original state. The numerical representation of images is a large matrix, where each element represents the status of a pixel in the image. Following image processing, it becomes possible to obtain the displacement field for every pixel within the image (Yoneyama and Murasawa, 2009). This procedure is illustrated in Figure 2.

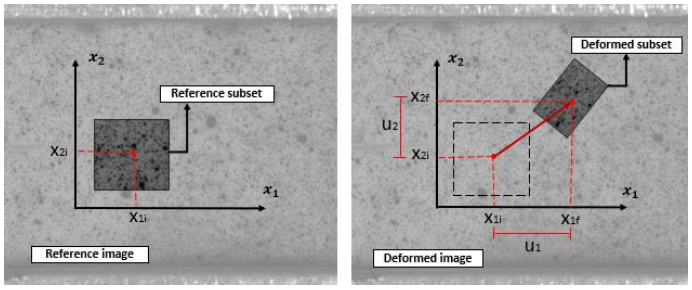


Figure 2. Schematic representation of the Digital Image Correlation technique.

### 2.3 Experimental setup

The pure shear specimens were subjected to a quasi-static mode I fracture loading, at room temperature (≅ 25°C), using a universal tensile machine, which was configured to move with a constant speed of 8 mm/min.

During tests, images were captured using a high-resolution Sony XCD-SX910 camera with a 10x MLH lens. The camera was positioned perpendicular to the flat surface of the specimen to capture images of the crack region, as shown in Figure 3. The image acquisition time was set at 0.5s and a 50 kgf load cell was used to measure load data simultaneously. The post-processing analysis was performed using the iCorrVision open-source DIC software (Filho et al., 2022). A calibration factor of 42.4 pixels/mm was considered.

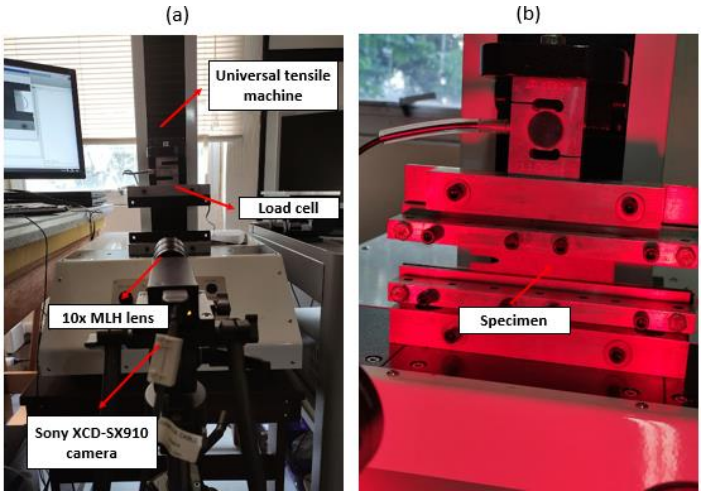


Figure 3. Experimental setup: hyperelastic material submitted to a mode I fracture loading.

## 3. MATHEMATICAL APROACH

### 3.1 Constitutive model

In the present work, an incompressible and isotropic hyperelastic material was used. The pure shear specimens had an initial crack of 20 mm, a small thickness and length approximately 8 times greater than the height, fixed at its lower part and pulled in the direction of its height, as shown in Figure 4. Thus, it can be admitted that the specimen is subjected to a plane stress state.

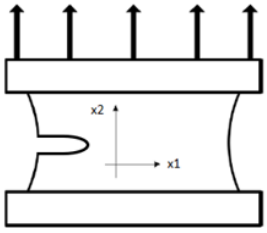


Figure 4. Representation of the test performed.

The displacement full-field is given by

$$\boldsymbol{u}(\boldsymbol{X},t) = \boldsymbol{x}(\boldsymbol{X},t) - \boldsymbol{X} \tag{1}$$

where $\boldsymbol{X}$ is the position of the body in the reference configuration, $\boldsymbol{x}$ is the position of the deformed body in the current configuration and $t$ is the time.

The material element, in the reference configuration $d\boldsymbol{X}$, is transformed to a material element $d\boldsymbol{x}$ in the current configuration, according to

$$\frac{d(\boldsymbol{u}+\boldsymbol{X})}{d\boldsymbol{X}} = \frac{d\boldsymbol{u}}{d\boldsymbol{X}} + \frac{d\boldsymbol{X}}{d\boldsymbol{X}} = \nabla\boldsymbol{u} + \boldsymbol{I} = \boldsymbol{F} \tag{2}$$

where $\boldsymbol{F}$ is the deformation gradient tensor, and $\boldsymbol{I}$ is the identity matrix.

Using the deformation gradient tensor expressed in Eq. (2), the left Cauchy-Green deformation tensor, $\boldsymbol{B}$, can be written as

$$\boldsymbol{B} = \boldsymbol{F}\boldsymbol{F}^T \tag{3}$$

The strain energy function, $W$, is a representation of the mechanical energy accumulation per unit volume in a deformed body. In the tests conducted, is assumed that the material maintains a constant volume and has uniform mechanical properties in all directions. As a result, the strain energy function can be expressed as a function of the material's invariants. In this work, the Yeoh (1993) strain energy model was used, which assumes independence from the second invariant, $I_2$. Therefore, $W$ can be written in terms of the first invariant only, i.e.,

$$W = W[I_1(\boldsymbol{B})] \tag{4}$$

where $I_1$ is obtained taking the trace of $\boldsymbol{B}$.

For incompressible and isotropic hyperelastic materials, the Cauchy stress tensor is given by the following equation,

$$\boldsymbol{\sigma} = -p\boldsymbol{I} + 2\frac{dW}{dI_1}\boldsymbol{B} \tag{5}$$

where $p$ is the Lagrange multiplier, and $\boldsymbol{I}$ is the identity matrix.

In the present work, the third order Yeoh model was chosen, that is given by

$$W = \sum_{n=1}^{3} C_{n0}(I_1 - 3)^n = C_{10}(I_1 - 3)^1 + C_{20}(I_1 - 3)^2 + C_{30}(I_1 - 3)^3 \tag{6}$$

where $C_{10}$, $C_{20}$ and $C_{30}$ are the materials parameters. In the present work, the values used were found in (Benevides, 2015) and are presented in Table 2.

Table 2. Silicon rubber parameters

| | |
|---|---|
| $C_{10}$ | 0,149 MPa |
| $C_{20}$ | 0,029 MPa |
| $C_{30}$ | 0,012 MPa |

### 3.2 J-Integral

When dealing with structures with the presence of plasticity, the conventional approach of linear elastic fracture mechanics does not provide an accurate analysis of material behavior. Consequently, it has become necessary to develop alternative methods of fracture mechanical analysis that account for nonlinear behaviors. Thus, Rice (1968) introduced the concept of J-Integral, which quantifies fracture toughness by evaluating the strain and stress fields around the crack tip using a closed path. In this study, the J-Integral was employed to analyze a hyperelastic material.

For two-dimensional strain fields of linear and nonlinear elastic materials, the line J-integral has the same value for any chosen path around the crack tip, and is given by

$$J = \int_{\Gamma} \left[ W\, dx_2 - \boldsymbol{T}\, \frac{\partial \boldsymbol{u}}{\partial \boldsymbol{X}} ds \right] \tag{7}$$

where $\Gamma$ is the closed path around the crack, which starts at the bottom of the crack and proceeds counterclockwise to its top; $\boldsymbol{u}$ is the displacement vector; $W$ is the strain energy density function, given by Eq. (6); $x_2$ is the direction perpendicular to the crack propagation; $\boldsymbol{T}$ is the vector representing the normal stresses to the boundary $\Gamma$, given by

$$\boldsymbol{T} = \boldsymbol{\sigma}\, \boldsymbol{n} \tag{8}$$

where $\boldsymbol{\sigma}$ is the Cauchy stress tensor, given by Eq. (5), and $\boldsymbol{n}$ is the normal vector to $\Gamma$.

Since the Digital Image Correlation technique uses a rectangular grid, in the present work, three rectangular paths were chosen, as shown in Figure 5.

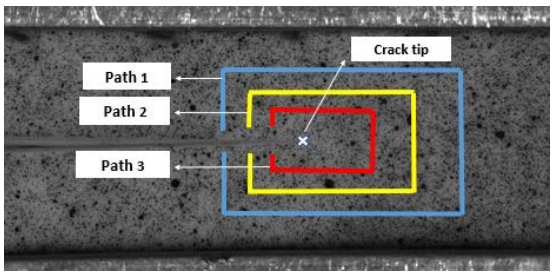


Figure 5. Paths used to evaluate the line J-Integral.

It has already been reported in literature that the calculation of the J-Integral using a contour surrounding the crack tip does not offer a high degree of precision and can be mathematically complex depending on the selected path (Becker et al., 2012). Li et al. (1985) proposed an equivalent expression in terms of the volume integral using the divergence theorem. This volume integral can be converted to an area integral in the case of two-dimensional problems. Thus, the area J-Integral is

$$J = \int_{A} \left( \sigma_{ij} \frac{du_i}{dX_1} - W \delta_{1j} \right) \frac{\partial q}{\partial X_j}\, dA \tag{9}$$

where $A$ is an area containing the crack tip; $\boldsymbol{u}$ is the displacement vector; $W$ is the strain energy density function, given by Eq. (6); $q$ is a function that imposes a translation in the $X_1$ direction on the material points inside the inner boundary, while the points on the outer boundary remain fixed, that is, it represents the virtual crack propagation; $\delta_{1j}$ is the Kronecker delta, defined as

$$\delta_{1j} = \begin{cases} 1, if\ j = 1 \\ 0, if\ j = 2 \end{cases} \tag{10}$$

In this work, three regions were chosen surrounding the crack tip to estimate the area J-Integral. These regions are presented in Figure 6.

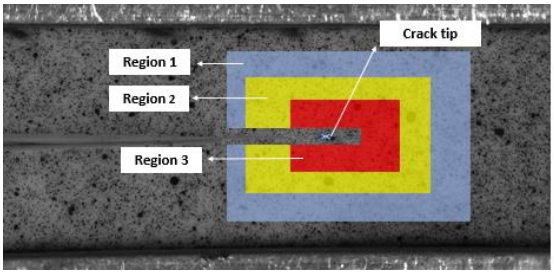


Figure 6. Regions used to evaluate the area J-Integral.

## 4. RESULTS AND DISCUSSION

Figure 7 presents a set of images that were captured during the tests, showing the crack propagation in a pure shear specimen submitted to a mode I loading.

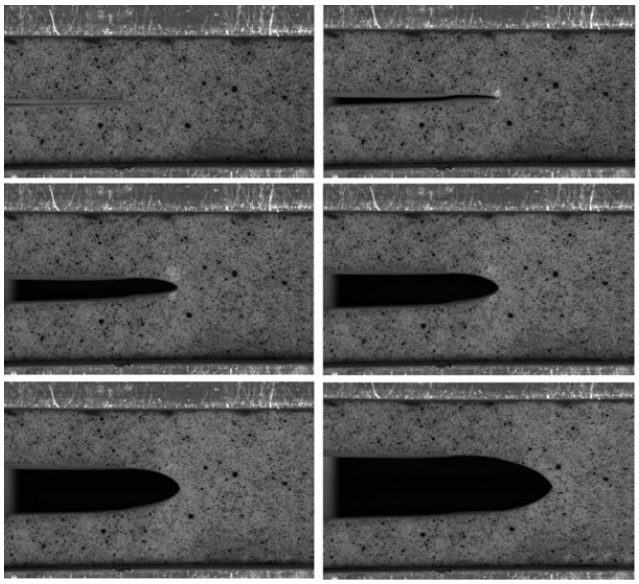

Figure 7. Crack propagation in the pure shear specimen.

Figure 8 illustrates full-field displacements $u_1$ and $u_2$, obtained from the Digital Image Correlation method, where it is possible to observe that the displacement $u_1$ is greater in the lower and upper regions of the crack, while in the region closer to the crack tip – central region of the material – the displacement $u_1$ approaches zero. It is also noted that the displacement $u_2$ is smaller in the lower part of the crack, where the material remains fixed during the test, and there is a gradual increase towards the upper region.

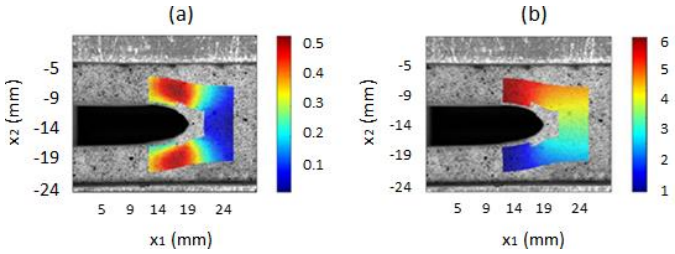


Figure 8. Displacement fields: (a) $u_1$ and (b) $u_2$.

By comparing the displacement fields, it is noted that the vertical displacement field $u_2$ is greater than horizontal displacement field $u_1$. This observation is in accordance with the expected behavior for mode I fracture loading. The dominance of $u_2$ can be attributed to the crack opening and propagation in the vertical direction.

Figure 9 shows the full-field strains and stresses. The distribution of stresses and strains provides valuable insights into the mechanical response of the material, particularly in the vicinity of the crack, supporting in understanding the fracture behavior. It is noteworthy that, despite performing a pure shear test, or planar test, a state of pure shear is not configured, due to the presence of the crack in the material. Thus, both normal stress and shear stress are present along the specimen.

From Figure 9, it is verified that the measured $e_{11}$ full-field strain is relatively small, when compared with $e_{22}$ and $e_{12}$, that is, $e_{11}$ is less influenced by the crack propagation. Analyzing $e_{22}$, it is possible to observe a more intense deformation at crack tip, due to the traction force that generates its propagation. In the case of $e_{12}$, it is noted that the presence of the crack induces an asymmetric deformation state around it.

Observing the stresses in Figure 9, a comparison between the values indicates that $\sigma_{22}$, i.e., the stress in loading direction, exerts a greater influence on the crack propagation. On the other hand, the stresses $\sigma_{11}$ and $\tau_{12}$ exert a lesser influence on its propagation. This suggests that the crack growth is primarily driven by the stress perpendicular to the crack plane, while the other stresses have a relatively smaller impact, as expected for the mode I loading.

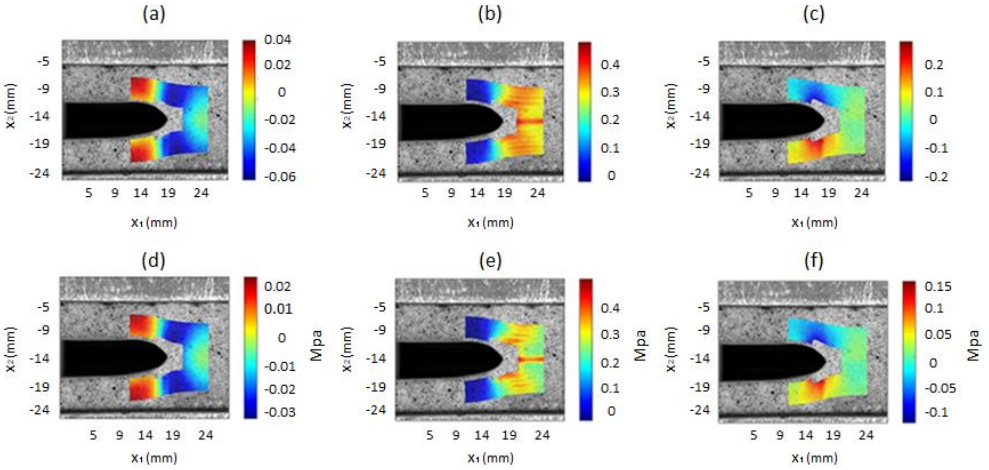


Figure 9. Strains (a) $e_{11}$, (b) $e_{22}$, (c) $e_{12}$ and stresses (d) $\sigma_{11}$, (e) $\sigma_{22}$ , (f) $\tau_{12}$ around the crack tip.

As discussed in the literature, the presence of a crack promotes a strain concentration around it. In order to validate that strain concentration, the Von Mises criterion was used (Titkov et al., 2018). Figure 10 shows the result obtained from the Von Mises equivalent stress, $\sigma_{eq}$. It is possible to see that $\sigma_{eq}$ is higher near the crack tip, illustrating the existence of a stress concentration area, as expected.

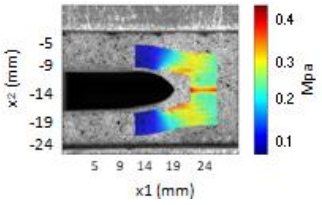


Figure 10. Equivalent Von Mises stress.

The estimation of the crack tip displacement, *da*, for all specimens was also carried out. To find this value, the Digital Image Correlation program was executed again, but considering a grid of 2x2 elements, positioned at the crack tip. In this process, the horizontal and vertical crack tip displacements, respectively $da_1$ and $da_2$, were obtained and used to evaluate the crack extension, as shown in Eq. (11). An alternative approach can be found in (Filho et al., 2022).

$$da = \sqrt{{da_1}^2 + {da_2}^2} \tag{11}$$

Figure 11(a) and 11(b) show the line J-Integral and area J-Integral curves as a function of the crack tip displacement, *da*, in millimeters. In these figures, the average and standard deviation values of J-integral were evaluated from three pure shear specimens.

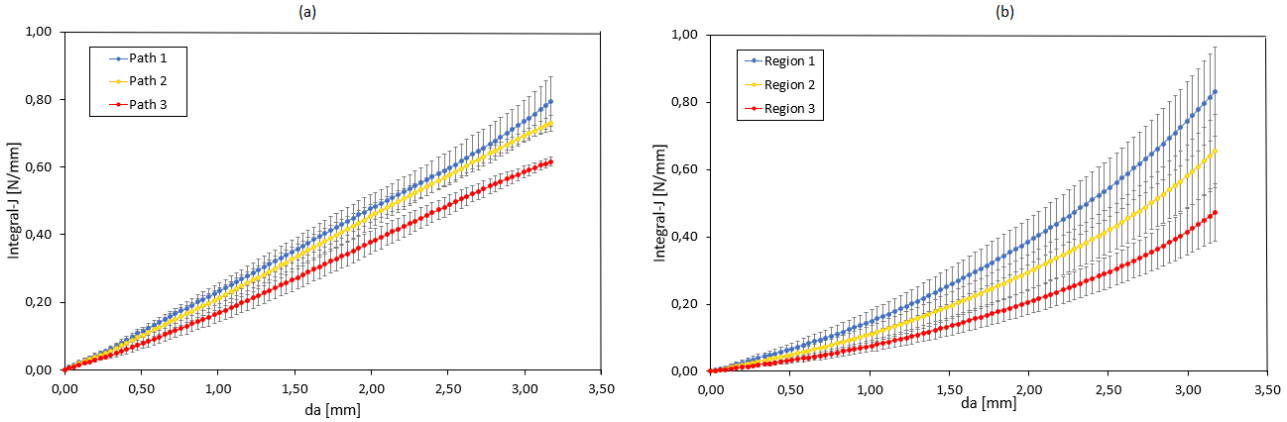


Figure 11. (a) Line J-Integral and (b) Area J-Integral versus the crack growth.

It is noted from Figure 11(a) that the values obtained using path 3 diverge significantly from the results obtained with paths 1 and 2. This difference can be attributed to the close proximity of path 3 to the crack tip, where the stress singularity has a pronounced influence. On the other hand, in Figure 11(b) is seen that the regions chosen does not coincide, as evidenced by the non-intersection of their respective error bars along the curves. That is, the regions chosen are still suffering influence from the stress concentration. This suggests that, in regions where the singularity of the crack tip does not have a substantial impact, the line J-integral and the area J-integral are independent of the chosen path/region.

These findings indicate the significance of the chosen path/region in the calculation of the J-integral and its sensitivity to the presence of the stress singularity at the crack tip. It is essential to consider these factors when experimentally computing the fracture toughness and characterizing the behavior of materials under different loading conditions. By carefully selecting an appropriate path/region, accurate assessments of fracture toughness and crack propagation can be achieved.

The Figure 12 illustrates the comparison between the line J-Integral and the area J-Integral, where the curves represent the average of the values obtained in each of the chosen paths/regions, and the error bars represent the standard deviation.

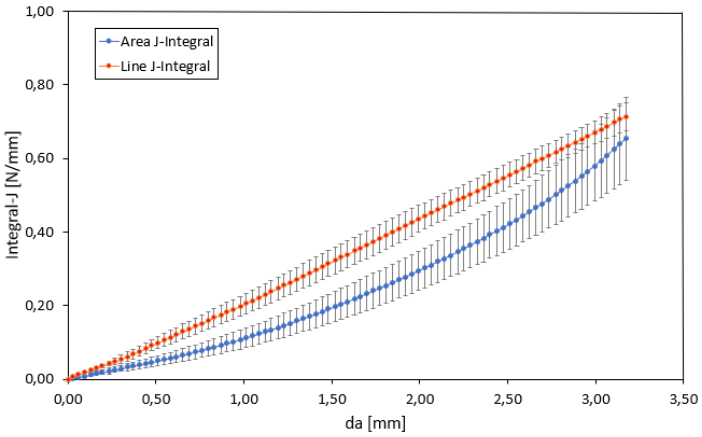


Figure 12. Comparison between Line J-Integral and Area J-Integral.

Although the values of the line and area J-Integral curves are close, they do not exhibit identical behavior. The area J-Integral curve displays a more pronounced nonlinear behavior compared to the line J-Integral curve. This result is expected due to the difference of domain between the line J-Integral and area J-Integral. Besides that, the deformation of the grid caused by crack propagation during the execution of the Digital Image Correlation method, leads to deviations in the obtained values.

As previously shown in Figure 9, by comparing the stresses $\sigma_{11}$ and $\tau_{12}$, it can be seen that the stress $\sigma_{22}$ has a greater influence on crack propagation. Therefore, an analysis was carried out to show the influence of the stress $\sigma_{22}$ in the calculation of the J-Integral. Thus, the calculation of the line and area J-Integral was performed, not considering the stresses $\sigma_{11}$ and $\tau_{12}$. The results are shown in Figure 13.

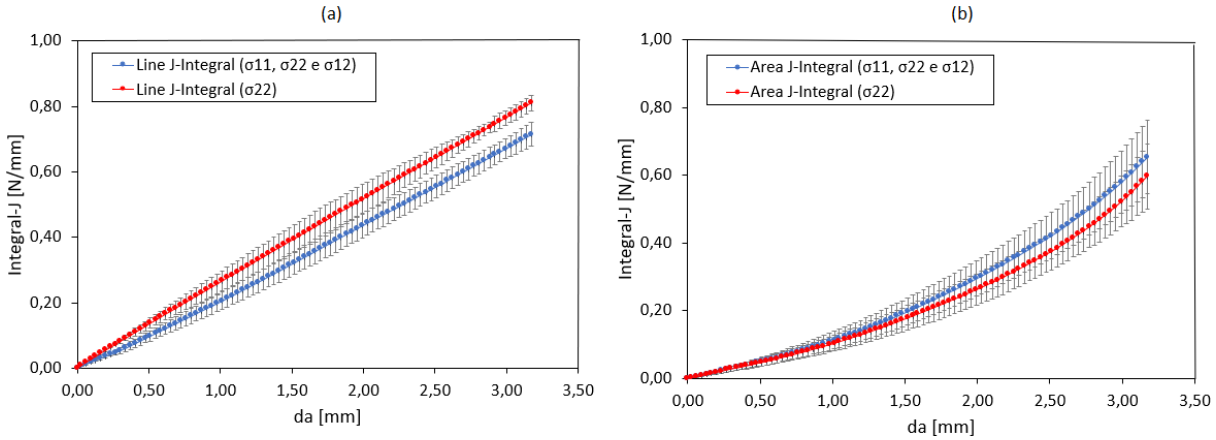


Figure 13. Influence of stress $\sigma_{22}$ in the calculation of the (a) Line J-Integral and (b) Area J-Integral.

According to the curves shown in Figure 13, the stress $\sigma_{22}$ has a great influence on the calculation of the line J-Integral and area J-Integral. It can be seen that the area J-Integral curves are closer than the line J-Integral curves. Therefore, the stresses $\sigma_{11}$ and $\tau_{12}$ could be removed from the area J-Integral study without compromising the results. In line J-Integral case, the existing difference between the curves can cause an error, so it is not possible to have the same conclusion.

In order to validate the obtained results of line and area J-Integral, the model proposed by Kim (1989) was used. This model is widely used for materials that undergo large deformations, such as elastomers, and it is based on the energy stored by the specimen during the fracture test. The J-Integral proposed by Kim is given by

$$J_{Kim} = \frac{U}{t_0(w_0 - a_0)} = \frac{\int_0^{\bar{x}} F\, d\bar{x}}{t_0(w_0 - a_0)} \tag{11}$$

where $t_0$ and $w_0$ are, respectively, the initial thickness and length of the specimen, and $a_0$ is the initial crack length. $U$ is the stored energy during the test, defined as the area under the loading versus displacement curve.

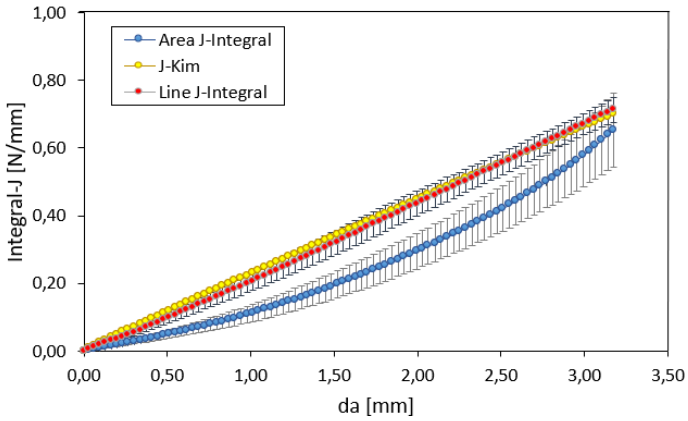


Figure 14. Comparison between Kim's model, Line J-Integral and Area J-Integral.

As can be seen in Figure 14, the curve obtained from Kim's model coincides with the line J-Integral curve throughout its entirety. However, when comparing the curve with the area J-Integral, it is evident that they exhibit different behaviors. Specifically, the area J-Integral curve demonstrates a more pronounced non-linear behavior compared to Kim's model.

This divergence in the behavior of the curves is considered normal and expected due to the difference in the calculation domains of the integrals. Additionally, the deformation of the grid used during the execution of the Digital Image Correlation method to obtain displacement fields introduces deviations in the obtained values.

## 5. CONCLUSION

In the present work, a study was carried out in a hyperelastic material submitted to a mode I fracture loading. The displacement fields were obtained through the Digital Image Correlation method, and the third order Yeoh hyperelastic model was used in J-Integral calculation.

It was observed that: the obtained displacement fields are consistent with the mode I fracture loading; stresses and strains are similar in the way they are distributed around the crack tip, indicating that the constitutive equation used is adequate to describe the hyperelastic behavior of the material used in this study.

The results obtained reveal that the line J-Integral and the area J-Integral do not have similar values, due to the difference in the domain they are calculated. It is possible to conclude that the stress $\sigma_{22}$ exerts a strong influence on the J-Integral calculation, so in area J-Integral case, the other stresses could be removed from the calculations without affecting the final outcome. Besides that, it is inferred that Kim's model and line J-Integral have the same value for paths far from the stress concentration in the crack tip.

## 6. REFERENCES

Becker T.H., Mostafavi M., Tait R.B., Marrow T.J., 2012. "An approach to calculate the J-integral by Digital Image Correlation displacement field measurement". *Fatigue & Fracture of Engineering Materials & Structures*, Vol. 35, p. 971-984.

Benevides R.O., 2015. *Mechanical behavior of silicone rubber reinforced with different concentrations of alumina nanoparticles (in Portuguese)*, Master thesis, Graduate Program in Mechanical Engineering, Universidade Federal Fluminense, Rio de Janeiro, Brazil.

Cianchetti, M., Laschi, C., Menciassi, A., and Dario, P., 2018. "Biomedical applications of soft robotics". *Nature Reviews Materials*, Vol. 3, p. 143–153.

Filho, J.C.A.D., Nunes, L.C.S., Xavier, J.M.C, 2022. "An Alternative Digital Image Correlation-Based Experimental Approach to Estimate Fracture Parameters in Fibrous Soft Materials". *Materials*, Vol. 15, p. 2413.

Filho, J.C.A.D., Nunes, L.C.S., Xavier, J.M.C, 2022 "iCorrVision-2D: An integrated python-based open-source Digital Image Correlation software for in-plane measurements (part 1)". *SoftwareX*, Vol. 19, p. 101131.

Griffith, A.A., 1921. "The phenomena of rupture and flow in solids". *Philosophical Transactions of the Royal Society of London*. Vol. 221, p. 582–593.

Horvath, M.A., Varela, C.E., Dolan, E.B., Whyte, W., Monahan, D.S., Payne, C.J., Wamala, I.A., Vasilyev, N.V., Pigula, F.A., Mooney, D.J., Walsh, C.J., Duffy, G.P., and Roche,E.T., 2018. "Towards Alternative Approaches for Coupling of a Soft Robotic Sleeve to the Heart". *Annals of Biomedical Engineering*, Vol. 46, p. 1534–1547.

Irwin, G.R., 1957. "Analysis of stresses and strains near the end of a crack traversing a plate". *Journal of Applied Mechanics*, Vol. 24, p. 361–364.

Khaniki, H. B., Ghayesh, M. H., Chin, R., and Amabili, M., 2022. "A review on the nonlinear dynamics of hyperelastic structures". *Nonlinear Dyn*, Vol. 110, p. 963–994.

Kim B.H., Joe C.R., 1989. "Single specimen test method for determining fracture energy of highly deformable materials". *Engineering Fracture Mechanics*, Vol.32, p. 155-161.

Kumar, P., and Ali syed, G.M., 2020. "Emerging trend in manufacturing of 3D biomedical components using selective laser sintering: A review". *E3S Web of Conferences*, Vol. 184, p. 1047.

Li, F.Z., Shih, C.F., Needleman, A., 1985. "A comparison of methods for calculating energy release rates". *Engineering Fracture Mechanics*, Vol. 21, p. 405-421.

Rice, J.R., 1968. "A Path Independent Integral and the Aproximate Analysis of Strain Concentration by Notches and Cracks". *Journal of Applied Mechanics*, Vol. 35, p 379-386.

Sutton, M.A., McNeill, S.R., Helm, J.D., Chao, Y.J., 2000. "Advances in two-dimensional and three-dimensional computer vision". *Photomechanics Topics in Applied Physics*, Vol. 77, p 323-372.

Sutton, M.A., Wolters, W.J., Peters, W.H., Ranson, W.F., McNeill, S.R., 1983. "Determination of displacement using an improved digital correlation method". *Image and Vision Computing*, Vol. 1, p. 133-139.

Titkov V.V., Eremin A.V., Panin S.V., Lyubutin P.S, Kozulin A.A., 2018. "Algorithm for J-Integral Measurements by Digital Image Correlation". *IOP Conference Series: Materials Science and Engineering*, Vol. 731, p. 12003.

Wells, A.A., 1963. "Application of fracture mechanics at and beyond general yielding". *British Welding Journal*, Vol. 10, p. 563-570.

Xiong, J., Chen, J., and Lee, P.S., 2021. "Functional Fibers and Fabrics for Soft Robotics, Wearables, and Human–Robot Interface". *Advanced Materials – Special Issue: Soft Robotics*, Vol. 33, p. 2002640.

Yeoh, O.H., 1993 "Some Forms of the Strain Energy Function for Rubber". *Rubber Chemistry and Technology*. Vol. 66, p. 754-771.

Yoneyama, S. and Murasawa, G., 2009. "Digital Image Correlation". *Experimental mechanics*, Vol. 207.

## 7. RESPONSIBILITY NOTICE

The author is the only responsible for the printed material included in this paper.